BASIC SCIENCE

Nanomedicine: Nanotechnology, Biology, and Medicine
24 (2020) 102109

Original Article

nanomedjournal.com

Synchronized Rayleigh and Raman scattering for the characterization of single optically trapped extracellular vesicles

Agustin Enciso-Martinez, Ir.[a], Edwin van der Pol, Dr.[b,c,d], Aufried T.M. Lenferink, Ing.[a], Leon W.M.M. Terstappen, Prof. Dr.[a], Ton G. van Leeuwen, Prof. Dr.[b,d], Cees Otto, Dr.[a,*]

[a]*Department of Medical Cell BioPhysics, TechMed Centre, University of Twente, Enschede, The Netherlands*
[b]*Department of Biomedical Engineering and Physics, Amsterdam University Medical Centers, Location AMC, University of Amsterdam, The Netherlands*
[c]*Laboratory Experimental Clinical Chemistry, Amsterdam University Medical Centers, Location AMC, University of Amsterdam, The Netherlands*
[d]*Vesicle Observation Center, Amsterdam University Medical Centers, Location AMC, University of Amsterdam, The Netherlands*

Revised 3 October 2019

Abstract

Extracellular Vesicles (EVs) can be used as biomarkers in diseases like cancer, as their lineage of origin and molecular composition depend on the presence of cancer cells. Recognition of tumor-derived EVs (tdEVs) from other particles and EVs in body fluids requires characterization of single EVs to exploit their biomarker potential. We present here a new method based on synchronized Rayleigh and Raman light scattering from a single laser beam, which optically traps single EVs. Rapidly measured sequences of the Rayleigh scattering amplitude show precisely when an individual EV is trapped and the synchronously acquired Raman spectrum labels every time interval with chemical information. Raman spectra of many single EVs can thus be acquired with great fidelity in an automated manner by blocking the laser beam at regular time intervals. This new method enables single EV characterization from fluids at the single particle level.

Key words: Extracellular vesicles; Exosomes; Raman spectroscopy; Single particle analysis; Nanomedicine; Nanoparticles

Recent studies have shown that small lipid-membrane-bound vesicles called Extracellular Vesicles (EVs) derived from cancer cells play a role in tumor cell proliferation, migration, invasion, and metastasis,[1–3] and the peripheral blood load of relatively large tumor-derived EVs is strongly associated with poor clinical outcome.[4] The EVs, which may be as small as 50 nm,[5] are able to transport proteins, nucleic acids and membrane components to neighboring or distant cells, influencing cellular behaviors. Hence, EVs derived from diseased cells, such as cancer cells, could trigger oncogenic signals and promote tumor development.[2] Tumor-derived extracellular vesicles (tdEVs) can be present in body fluids, such as blood.[6–10] However, their identification and characterization are challenging due to their heterogeneity, ultra-small size, low refractive index, size overlap with physiological EVs and contaminants in body fluids, and the lack of knowledge on their chemical composition. Specially, their broad size range overlaps not only with non-tdEVs, but also with lipoproteins and protein aggregates that fall in the EV size range.[11] Thus, the ensemble average inherent to bulk analysis methods requires a sensitivity which techniques like ELISA or western blot unlikely have. Single particle analysis may overcome this problem and pave the road towards identification of rare tdEV populations.

There are well established methods for single particle analysis, such as nanoparticle tracking analysis (NTA), resistive pulse sensing and flow cytometry that together can provide the size, number, concentration, electrophoretic mobility and refractive index of EVs. However, these methods fail in providing information on the chemical composition of EVs, which is essential to identify their origin. In recent years, Raman spectroscopy (RS) has been used to contribute chemical information of EVs and tdEVs.[12–17] RS is a label-free chemical

Funding: This work is part of the Perspectief Program Cancer ID [14193], which is in part financed by the Netherlands Organization for Scientific Research–Domain Applied and Engineering Sciences (NWO-TTW). Part of this work was supported by the VENI program [15924, E. van der Pol] of the Netherlands Organization for Scientific Research–Domain Applied and Engineering Sciences (NWO-TTW).

*Corresponding author at: University of Twente, 7500 AE Enschede, The Netherlands.

E-mail addresses: a.encisomartinez@utwente.nl, (A. Enciso-Martinez), e.vanderpol@amsterdamumc.nl, (E. van der Pol), l.w.m.m.terstappen@utwente.nl, (L.W.M.M. Terstappen), t.g.vanleeuwen@amsterdamumc.nl, (T.G. van Leeuwen), c.otto@utwente.nl. (C. Otto).

https://doi.org/10.1016/j.nano.2019.102109

characterization technique based on the inelastic scattering of light by molecules. RS combined with optical tweezers, provides Raman spectra of particles trapped in the focal spot. Pioneered by Ashkin,[18,19] optical tweezers use a diffraction limited beam to stably trap a particle in three dimensions. Particles in Brownian motion that enter the trapping focal spot experience a net force that brings them to the axial center of the laser beam waist slightly displaced form the focal plane.

Previous studies demonstrate trapping of single solid particles in the size range of EVs, such as silica beads, polystyrene beads and viruses.[20,21] The trapping of single particles has been complemented with characterization techniques such as fluorescence spectroscopy[22] and Raman spectroscopy.[23] Although EVs have also been studied with Raman, single EV Raman measurements have never been experimentally confirmed. Indirect evidence has been used in some studies to presume single EV or liposome trapping and chemical characterization.[13,14,17,24] However, the unequivocal proof that a trapping event involves a single EV and the ability to trap EVs at sufficiently high rates has not yet been shown.

Here, we propose a new method to optically trap single EVs and simultaneously disclose their inherent chemical composition by means of RS. The method distinguishes individual particle trapping events by the detected Rayleigh scattered light while synchronously measured Raman spectra enable the chemical characterization of individual EVs. Rayleigh scattering and Raman scattering are, respectively, elastic and inelastic scattering of light by particles in a medium. Further, our method involves a purge of the optical trap at regular time intervals. Hence, long time series of Rayleigh–Raman scattering events can be acquired starting each time from an empty trap. In this way, many individual trapping events can be acquired in an automated manner. Our method can be directly applied to diluted EV samples and does not require any EV isolation steps. The Raman spectra of multiple individual EVs enable a chemical fingerprint of the sample. We introduce and validate the method with polystyrene (PS) and silica (Si) beads. Subsequently, we show that synchronous Rayleigh–Raman scattering enables the identification of single EVs on the basis of the Raman spectral signature, which is related to their molecular composition.

Methods

PC3-derived EVs

PC3 cells provided by the American Type Culture Collection (ATCC) were used as a model to produce prostate cancer-derived EVs. Cells were cultured at 37 °C and 5% CO2 in RPMI-1640 with L-glutamine medium (Lonza, Cat. No.: BE12-702F) supplemented with 10% (v/v) fetal bovine serum (FBS), 10 U/mL penicillin and 10 μg/mL streptomycin. The initial cell density was 10,000 cells/cm^2 as recommended by the ATCC. Medium was refreshed every second day. At 80 to 90% confluence, cells were washed three times with phosphate buffer solution (PBS) and cultured in FBS-free RPMI-1640 with L-glutamine medium (Lonza, Cat. No.: BE12-702F) supplemented with 1 U/mL penicillin and 1 μg/mL streptomycin. After 2-3 days of cell culture, cell supernatant was collected in a 15 mL tube (Cellstar® tubes, Greiner Bio-one) and centrifuged at 800 ×*g* at room temperature for 10 min (Centrifuge 5804, Eppendorf) . The pellet containing dead or apoptotic cells and large cell fragments was discarded. The collected supernatant containing PC3-derived EVs was stored in aliquots of 500 μL (Micro tube 0,5 mL, PP, SARSTEDT) at −80 °C. Samples were thawed in a water bath at 37 °C before use. EV size distribution was determined using NTA (NanoSight NS500). An EV concentration of 1.9×10^9 particles/mL with a mean diameter (± standard deviation) of 157 (± 79) nm was found (Figure S1).

Polystyrene (Ps) and silica (Si) beads

To validate our technology, we used NIST traceable polystyrene (PS) beads (Nanosphere; Thermo Fisher, Waltham, MA, USA) with mean diameters of 100, 125, 147, 296 and 799 nm and plain silica (Si) beads (Silica Kisker, Steinfurt, Germany) with mean diameters of 182, 315, 405 and 548 nm. The concentration was determined by NTA (NS500, Malvern, UK). Diameters of the silica beads were obtained by TEM. The corresponding refractive indices of PS and Si beads are 1.586 and 1.464, respectively. The suspensions of beads were diluted in MilliQ to a concentration of 3×10^8-3×10^9 particles/mL to optimize the single particle trapping rate. PS and Si particle suspensions were vortexed for 3 s and re-suspended 3 times before experiments to prevent particle aggregation that may have occurred during storage. A suspension of 50 μL of each monodisperse sample of beads was then used for synchronous Rayleigh and Raman scattering measurements.

Sample preparation

PS beads, Si beads, and EVs derived from PC3 cells were used in a concentration of 3.6×10^8-5×10^{10} particles/mL and diluted in MilliQ (beads) or PBS (EVs) to this concentration if necessary. A 50 μL suspension of each particle type was placed on a well glass slide (BMS Microscopes; 1.0-1.2 mm thick, Cat. no.: 12290). The sample was covered with a glass cover slip (VWR Ltd, thickness No. 1, diameter: 22 mm, Cat. no.: 631-0158) and sealed with glued (EVO-STIK, Impact) onto the well glass slide (Figure 1, *A*). The glue was then cured at room temperature for ~30 min. The closed well glass slide was placed on the microscope table under the objective of the Rayleigh–Raman spectrometer.

Optical setup and measurements

The Rayleigh–Raman spectrometer is based on a home-built Raman spectrometer integrated with the base of an upright optical microscope (Olympus BX41). A single laser beam from a Coherent Innova 70C laser (λ_{exc}=647.089 nm) was used for optical trapping and illuminating beads and EVs. Rayleigh and Raman scattering was collected with a cover glass corrected dry objective (Olympus, 40×, NA: 0.95). Rayleigh and Raman scattering was separated in a homebuilt spectrometer and simultaneously detected with a single CCD camera. The spectrometer had an average dispersion of ~2.3 cm^{-1} (0.11 nm) wavenumber per pixel over the CCD camera surface with 1600 pixels along the dispersive axis and 200 pixels perpendicular to this axis. The spectral resolution was ~3.0 cm^{-1}. The laser

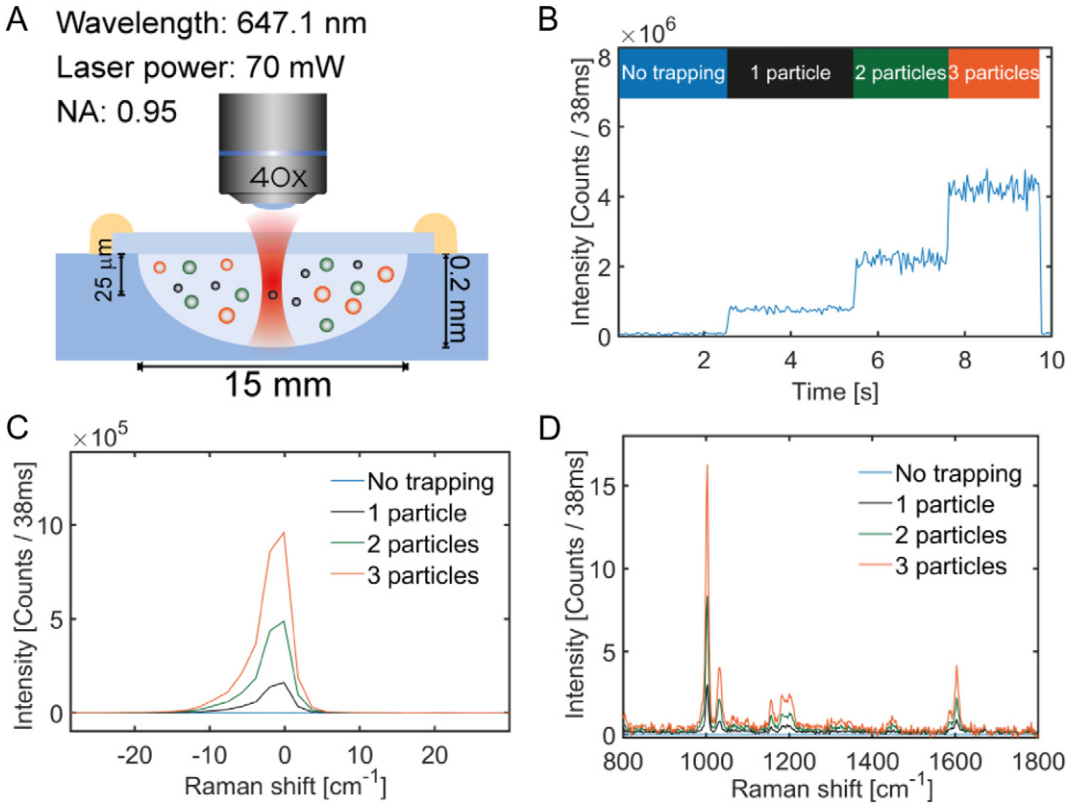

Figure 1. (**A**) Schematic overview of the setup. Particles in suspension are loaded in a well glass slide that is mounted under a microscope objective. (**B**) Rayleigh scattering intensity versus time clearly shows trapping of single PS beads (Ø=125 nm). Color labels at the top in (**B**), indicating the number of particles in the trap, correspond to the color of the traces in (**C**) and (**D**). (**C**) Intensity versus Raman shift for Rayleigh scattering without trapped particles, or with 1, 2 and 3 particles being trapped. (**D**) Raman scattering signals when no particle is trapped and when one, two and three particles are trapped in the laser focal spot.

power was measured underneath the objective and adjusted to 70 mW. By moving the objective along the z-axis, the laser focal spot is focused inside the solution, ~37 µm below the cover slip. The focal spot has a theoretical diameter of 370 nm and a Rayleigh range of 1160 nm based on full width half maximum. Rayleigh and Raman scattering spectra were typically acquired 256 times with an acquisition time of 38 ms over a period of ~9.7 s. The trapped particles were then released from the optical trap by blocking the laser beam with a shutter for ~1 s. This measurement cycle was repeated, typically, 100 times, which resulted in 100×256 = 25,600 Rayleigh–Raman spectra per measurement.

Backscattering calculations

Light scattering calculations based on Mie theory were used to relate the measured backscattering to the diameter and refractive index of PS and Si beads. The Rayleigh scattering intensity was compared with Mie scattering calculations of the intensity averaged over the collection angle of the microscope objective as a function of particle diameter. From these measurements it was theoretically predicted that with the present embodiment of the setup the Rayleigh light scattering signal was sufficiently intense to detect trapping of individual EVs, in spite of the small refractive index difference of EVs (n=1.37)[25] from water (n=1.33). We use the Mie scripts of Mätzler[26] in MATLAB (2018b, MathWorks, USA) to calculate the amplitude scattering matrix elements, which describe the relation between the incident and scattered field amplitudes of a sphere. Our model incorporates particle diameter and refractive index (RI), RI of the medium, the illumination wavelength, and the numerical aperture of the microscope.

Results

Brownian motion of EVs in suspension occasionally brings the EVs sufficiently close to the trap to experience a net trapping force directing towards the focal spot. Once an EV is trapped, an intense increase in the amplitude of the Rayleigh light scattering occurs, and this can be seen as a discrete step in a time trace (Figure 1, *B*). Such time trace results from the integration of the Rayleigh band over 50 pixels around 0 cm^{-1} plotted over time. As long as the shutter to the laser remains open, successive trapping and accumulation of particles occur until the focal volume becomes saturated with particles. Hence, monitoring the time trace over prolonged time enables to distinguish between zero (baseline), single (first step) and multiple trapping events, which can be enumerated (Figure 1, *B* and *C*). Synchronous acquisition of Raman spectra with the Rayleigh scattering allows us to assign a Raman spectrum to individual particles trapped (Figure 1, *D*). Purging the laser focus from trapped particles at

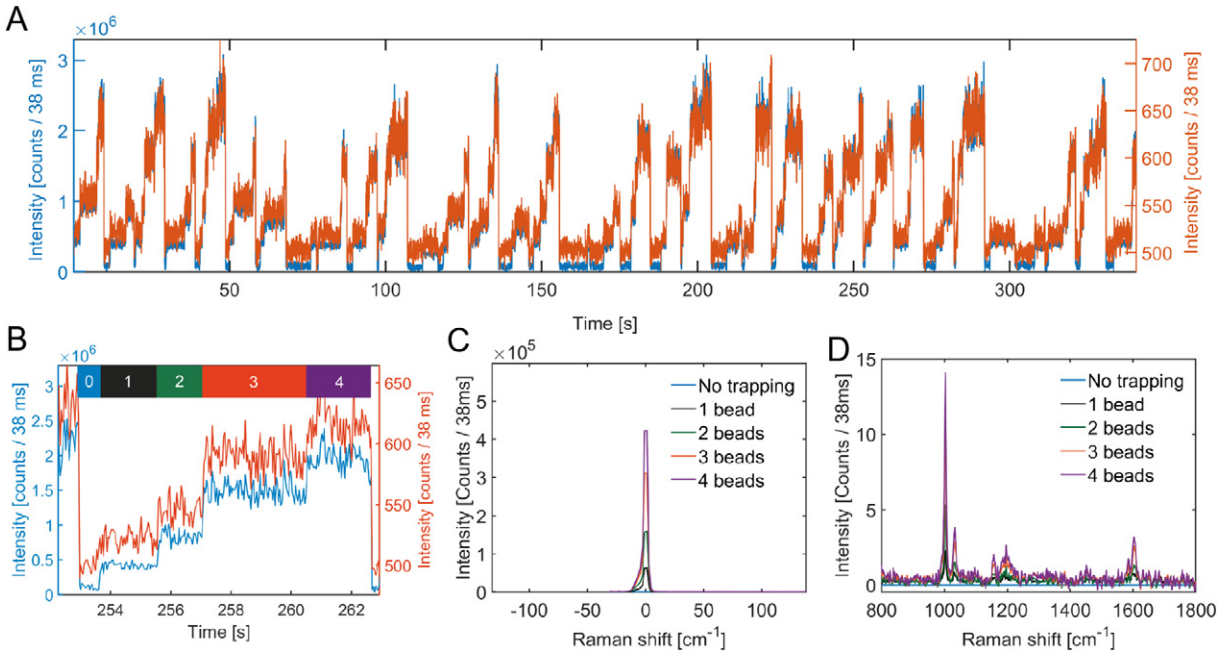

Figure 2. Rayleigh and Raman scattering signals of PS beads (Ø=100 nm). (**A**) Time trace of 35 cycles of Rayleigh (blue) and Raman (orange) scattering signals. This dataset contains 35×256 = 8960 spectra. (**B**) Magnified cycle from (**A**) to highlight the coincidences in the time traces of both, Rayleigh and Raman scattering signals for 4 trapping events (labeled as 0,1,2,3 and 4), with (**C**) and (**D**) showing the corresponding Rayleigh and Raman scattering signals.

regular time intervals enables the acquisition of many single EV trapping events in an automated manner over long periods of time, thus monitoring the composition of a suspension of EVs on the level of individual, single EVs with fidelity. Rayleigh and Raman scattering spectra were typically acquired 256 times with an acquisition time of 38 ms over a total period of ~9.7 s per cycle. After purging the laser focus a new cycle started.

To validate our technology, single PS and Si beads of various sizes (SI) were optically trapped and synchronous Raman acquisition was performed. To increase the event throughput of our Rayleigh–Raman setup we have automated the trapping and release of particles by acquiring both Rayleigh and Raman scattering signals overtime while closing a laser shutter to purge the trap from particles. Subsequent opening of the shutter starts another cycle of trapping events from an empty trap. For example, Figure 2, *A* shows the intensity time traces of both, the Rayleigh and the Raman scattering signals of 100 nm polystyrene beads. Integrating the characteristic 1003 cm^{-1} polystyrene Raman peak and plotting the intensity versus time result in a step-wise time trace that correlates with the Rayleigh time trace. This correlation confirms that the trapped particles indeed are polystyrene beads.

Figure 2, *B* shows a magnification of a part of the time trace in Figure 2, *A*. In the absence of particles in the laser focus, both scattering signals show a constant baseline. Trapping events can easily be observed from stepwise increases in the amplitude of the scattering signals. These signals increase upon the arrival and trapping of the first, second, third and fourth bead (labeled as 1, 2, 3 and 4, respectively in Figure 2, *B*). The average Rayleigh signal per time interval (0, 1, 2, 3 and 4 in Figure 2, *B*) is shown in Figure 2, *C*. Synchronous Raman acquisition labels each time interval with a Raman spectrum. The average Raman spectra of polystyrene for the five time intervals in Figure 2, *B* are shown in Figure 2, *D*.

The discrete nature of the time traces can be better visualized by segmenting all the levels in the Rayleigh signal and plotting the median value of each level versus time, as shown in Figure 3, *A*. Here, the time trace corresponds to the trapping and release of polystyrene beads with a diameter of 125 nm. The median values of each level in the Rayleigh intensity time traces are represented with a triangle. Figure 3, *B* shows a typical boxplot with a low standard deviation of the Rayleigh scattering intensities corresponding to the discrete trapping of beads. Five levels of scattering can be identified, namely the baseline (no trapped beads), and the first, second, third and fourth step or trapping event. Figure 3, *C* (black squares and red circles, right axis) shows the experimentally obtained backscatter intensity of the PS (n=1.586) and Si (n=1.464) beads in water (n=1.3317) versus their diameter. The backscatter intensity values correspond to the amplitude of the Rayleigh scattering for the first trapping events (e.g. blue box in Figure 3, *B*). These values have been plotted versus diameter and theoretically described by Mie theory, taking into account the diameter and refractive index of the beads as well as the optical configuration of the setup. Mie theory predicts an angle-dependent oscillatory behavior of the scattering cross section (Figure 3, *C*, left axis) for the collected backscattered light.

After developing and validating a procedure to trap single beads and measuring their Rayleigh scattering and Raman spectrum, we proceeded to investigate suspensions of EVs derived from a prostate cancer cell line (PC3 EVs) by synchronized Rayleigh–Raman scattering. Their intensity time traces are shown in Figure 4, *A*. The associated Raman scattering time trace was obtained from the integration of the lipid-protein band in the

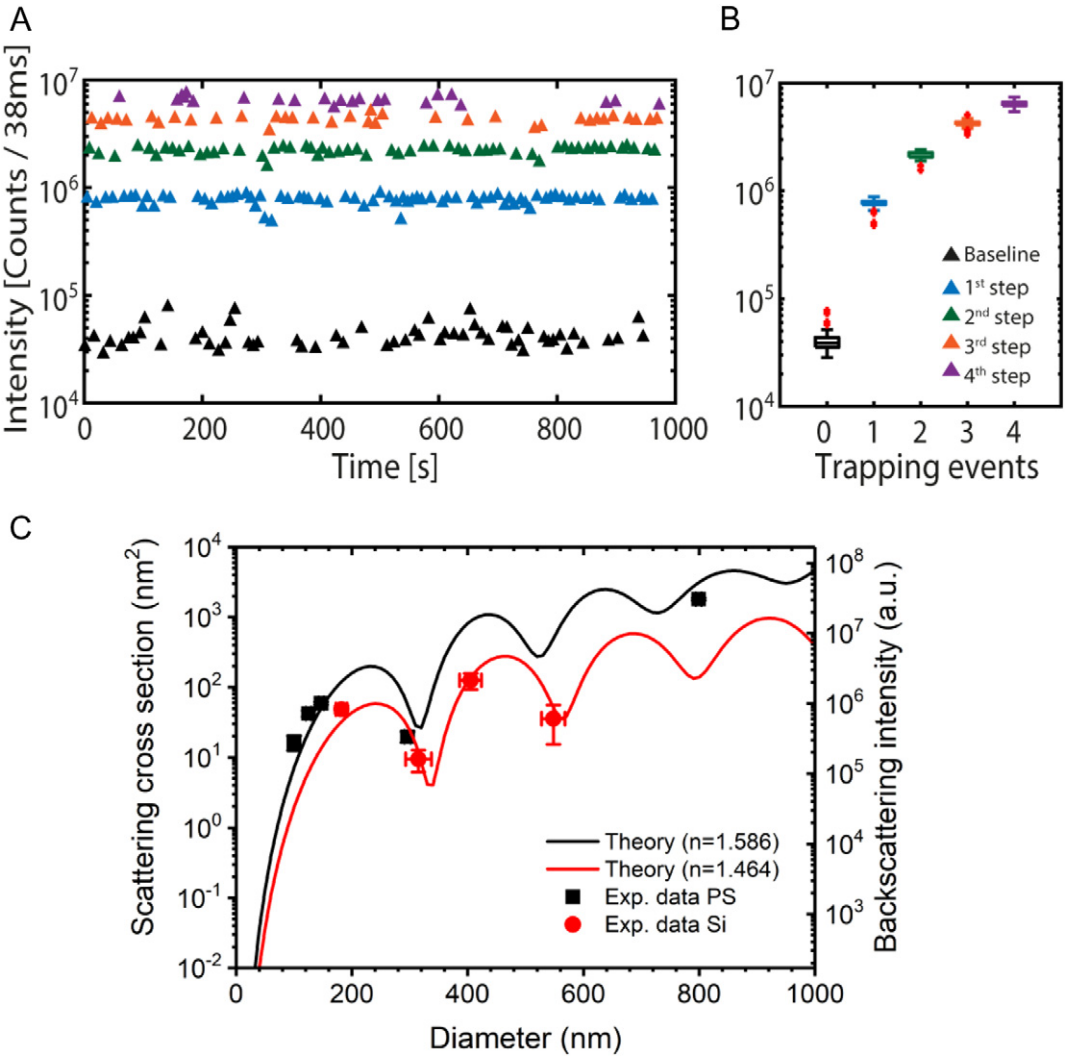

Figure 3. (**A**) Rayleigh scattering intensity of PS beads (Ø=125 nm), after time trace segmentation, and (**B**) its corresponding boxplot. (**C**) Prediction of the back-scattered signals (lines) from PS beads (black) and Si beads (red). The left vertical axis depicts the cross-section and the right vertical axis depicts the counts per 38 ms. Vertical error bars are SD of measured amplitudes. Horizontal error bars are SD of size distributions as provided by manufacturer.

Raman spectrum between 2811 cm^{-1} and 3023 cm^{-1}. The Rayleigh and Raman time traces show synchronous steps associated with trapping events and provide a tool to confirm the presence of a single EV in the trap. The mean Rayleigh intensity for PC3 EVs is 1.74×10^5 with an SD of 1.6×10^5 (n=94). Figure 4, *B* shows a magnified portion of the time trace in Figure 4, *A* with four time intervals labeled as 0, 1, 2, 3 and 4, corresponding to no trapping, first, second, third and fourth trapping events, respectively. The synchronously measured Raman spectra are extracted from the time trace and correspond to the Raman fingerprint of the particles trapped at the respective time intervals. Figure 4, *C* shows the Raman spectra of four different single PC3 EVs that correspond to the four time intervals presented in Figure 4, *B*.

To obtain a Raman fingerprint of PC3 EVs, we segmented the first particle trapping events from the Rayleigh time traces and thus obtained the time intervals where individual EVs generated a Raman spectrum. Figure 4, *D* shows the mean Raman spectra after baseline correction and noise removal for 94 PC3 EVs. Typical lipid and protein bands are shown at 1004, 1128, 1300, 1340, 1443, 1607, 1636-1690 cm^{-1}, as well as in the high frequency region between 2811 and 3023 cm^{-1}. Among other Raman peaks found in PC3 EVs are: 1247 (Amide III)[27] and 1663 (DNA and Amide I of proteins)[27], further confirming the trapping of EVs.

Discussion

Identification and characterization of a sub-population of EVs (e.g. tdEVs) require a method working at the single EV level. To achieve this, optical trapping and subsequent chemical characterization by Raman spectroscopy have been shown to be an attractive approach, because it is essentially a label-free approach that requires minimal sample preparation and enables chemical characterization of EVs in fluids. However, previous studies

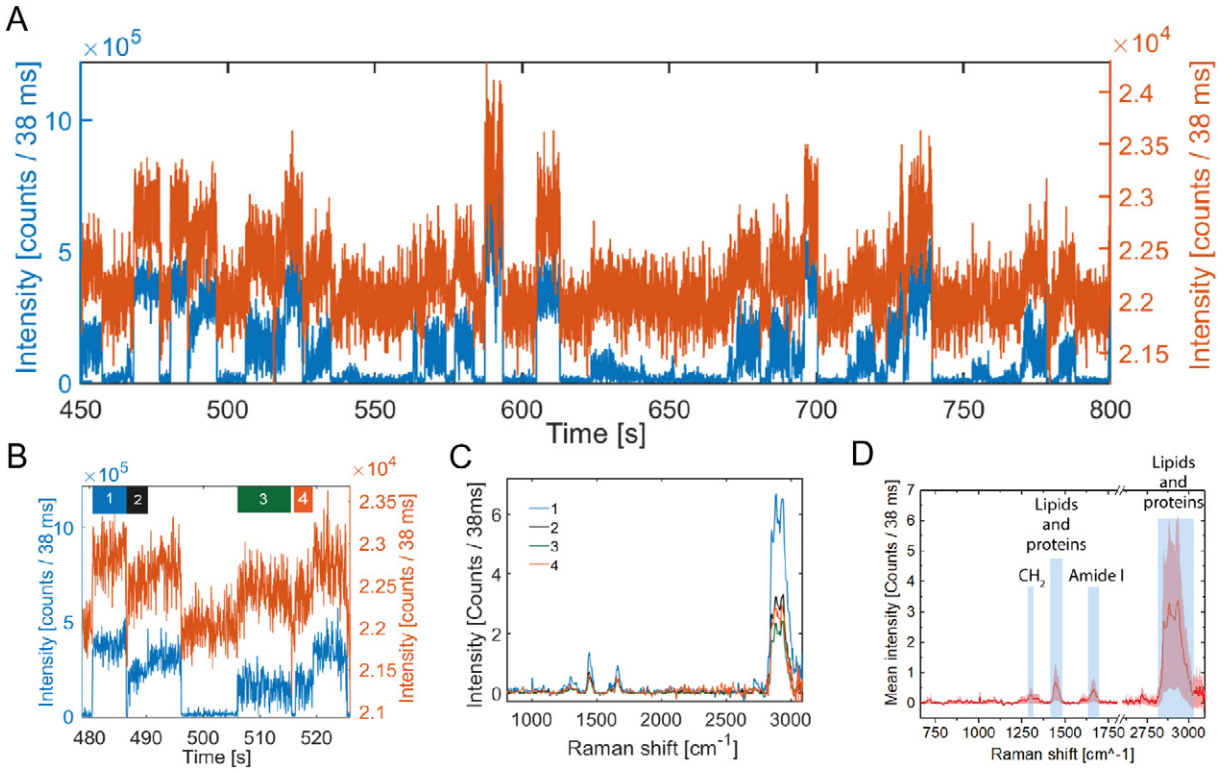

Figure 4. Rayleigh and Raman scattering signals of PC3 EVs. (**A**) Time trace of Rayleigh (blue) and Raman (orange) scattering signals. This dataset contains 100 cycles × 256 = 25,600 spectra. (**B**) Magnified cycle from (**A**) indicating 4 time intervals with single trapped PC3 EVs (labeled as 1, 2, 3 and 4), whose corresponding Raman spectra are shown in (**C**). (**D**) Mean Raman spectrum (thick line) and SD (shaded area) for 94 PC3 EVs.

have shown that Raman spectroscopy requires long integration times of many seconds up to minutes,[13–17] leading to the problem of trapping multiple particles. One option is to decrease the concentration of EVs and avoid any multiple trapping events, but the disadvantage is that at such low concentrations the chance of actually trapping an EV of interest, such as tdEVs, becomes low, and the acquisition of a sufficient large number of Raman spectra from single EVs may take many hours.

In this study, we have successfully investigated a new approach of synchronized Rayleigh and Raman scattering that enables to measure Raman spectra of single EVs from samples with 1.9×10^9 EVs/mL at a reasonably high trapping rate. In this approach, the Rayleigh scattering was used to detect the arrival of each individual particle in the trap from a large increase in the Rayleigh scattering signal. Synchronously, the Raman scattering signal was obtained with the same acquisition time as the Rayleigh scattering signal. Integration over the lipid-protein high frequency band enabled to obtain Raman time traces that coincide with the Rayleigh time traces. The time synchronicity is essential to enable an unequivocal relation between single EV trapping events visualized with Rayleigh scattering and the characteristic Raman fingerprint of that EV.

In order to establish the method of synchronous Rayleigh–Raman scattering, we first measured PS and Si beads in suspension. PS and Si beads with a refractive index of 1.586 and 1.464, and a diameter down to 100 nm and 182 nm, respectively, were easily trapped. Individual trapping events could be detected (Figure 2) and the time-synchronized Raman scattering assigned the familiar polystyrene spectrum to each PS particle. Mie theory was used to predict the scattering cross section of single PS and Si beads of different sizes. The prediction is in agreement with the experimental backscatter intensity values obtained from optically trapped single PS and Si beads.

Unlike PS and Si beads, EVs have a lower refractive index (1.35-1.40),[25,28–31] making their refractive index contrast small with respect to the aqueous solution with a refractive index of 1.3317. Such small refractive index contrast also results in a decrease of the trapping force. However, we were able to trap and identify single PC-3 EVs from a sample containing EVs with a diameter of 157 (± 79) nm, according to NTA. In addition, the low integration time (38 ms) and subsequent automated data analysis allowed the identification of single EVs in the focal spot and Raman spectra acquisition from approximately 400 single-EVs per hour. The signal processing that we have implemented automated the computation of Raman and Rayleigh time traces and segmented the step-wise signal to identify single and multiple trapping events with their respective Raman spectra.

Previous studies have claimed single EV trapping based on an increase of the Raman scattering signal.[14,15,17] Our approach integrates the Rayleigh scattering signal as a way to monitor and prove the trapping of single EVs. This enables the identification of smaller particles as the Rayleigh signal is much stronger (× ~10^3 to 10^4) than Raman scattering, whose weak scattering process can miss the detection of very small particles. Our method has the additional advantage of identifying single EVs irrespective of their Raman spectra due to the fact that it does not

rely on thresholding of a characteristic Raman peak or band integration. This becomes critical when trying to identify rare EV populations within a mixture of many other EV types. While the Rayleigh scattering signal allows the detection of single particles irrespective of their chemical composition, the Raman signal is used to identify the type of particles trapped. Other studies have relied on fluorescence signal to identify single EVs.[13] Immunostaining can disclose molecular-specific information, but it complicates sample preparation and workflow and requires specific markers to be used for rare EV populations. Our method is label-free and does not require additional steps to disclose the chemical information of an EV from its medium.

Although label-free Raman spectroscopy is not specific to molecules, the global information in Raman spectra enables to differentiate among different vesicles as previous studies of non-labeled EVs have demonstrated.[13–16] Our results show that the spectral region between 2811 and 3023 cm^{-1}, assigned to proteins and lipids, is the highest Raman intensity band for EVs (around 3× higher than the highest peak in the fingerprint region for PC3 EVs). This region in the Raman spectrum between 2811 and 3023 cm^{-1} enables an identification of different types of small single EVs and eventually tdEVs in plasma from cancer patients. The throughput of our technique can still be improved, e.g. by increasing the length of the time traces.

In conclusion, by synchronous acquisition of Rayleigh and Raman light scattering during optical trapping of sub-micrometer particles in suspension, we have been able to identify single trapping events at a high rate. This method could allow the identification of rare populations of EVs, such as tdEVs, where otherwise the ensemble average occludes the signal from single rare EVs. The synchronized detection of Rayleigh–Raman scattering and the ability to characterize single individual nanoparticles open a vast number of applications in different fields, e.g. identification of micro-plastics in contaminated water, virus detection, atmospheric science and catalysis[23], among others.

Appendix A. Supplementary data

Supplementary data to this article can be found online at https://doi.org/10.1016/j.nano.2019.102109.

References

1. Vader P, Breakefield XO, Wood MJA. Extracellular vesicles: emerging targets for cancer therapy. Trends Mol Med [Internet]. 2014;20(7):385–93. Available from: doi:10.1016/j.molmed.2014.03.002.
2. Katsuda T, Kosaka N, Ochiya T. The roles of extracellular vesicles in cancer biology: toward the development of novel cancer biomarkers. *Proteomics* 2014;**14**(4–5):412-25.
3. Kanada M, Bachmann MH, Contag CH. Signaling by extracellular vesicles advances cancer hallmarks. Trends in Cancer [Internet]. 2016;2(2):84–94. Available from: doi:10.1016/j.trecan.2015.12.005.
4. Nanou A, Zeune LL, de Wit S, Miller MC, Punt CJ, Groen HJM, et al. Tumor-derived extracellular vesicles in blood of metastatic breast, colorectal, prostate and non-small cell lung cancer patients associate with worse survival. In: AACR 2019 Proceedings: Abstract 4464 - American Association for Cancer Research [Internet]. 2019 [cited 2019 May 27]. Available from: https://books.google.nl/books?id=2CePDwAAQBAJ&pg=PT1982&lpg=PT1982&dq=Tumor-derived+extracellular+vesicles+in+blood+of+metastatic+breast,+colorectal,+prostate+and+non-small+cell+lung+cancer+patients+associate+with+worse+survival&source=bl&ots=qaCaW8WrEI&s.
5. Brisson AR, Tan S, Linares R, Gounou C, Arraud N. Extracellular vesicles from activated platelets: a semiquantitative cryo-electron microscopy and immuno-gold labeling study. Platelets [Internet]. 2017 Apr 3 [cited 2019 May 9];28(3):263–71. Available from: https://www.tandfonline.com/action/journalInformation?journalCode=iplt20.
6. Zwicker JI, Liebman HA, Neuberg D, Lacroix R, Bauer KA, Furie BC, et al. Tumor-derived tissue factor-bearing microparticles are associated with venous thromboembolic events in malignancy. Clin Cancer Res [Internet]. 2009 Nov 15 [cited 2017 Nov 23];15(22):6830–40. Available from: http://clincancerres.aacrjournals.org/cgi/doi/10.1158/1078-0432.CCR-09-0371.
7. Li J, Sherman-Baust CA, Tsai-Turton M, Bristow RE, Roden RB, Morin PJ. Claudin-containing exosomes in the peripheral circulation of women with ovarian cancer. BMC Cancer [Internet]. 2009 Jul 20 [cited 2017 Nov 23];9(1):244. Available from: http://bmccancer.biomedcentral.com/articles/10.1186/1471-2407-9-244.
8. Coumans FAW, Doggen CJM, Attard G, de Bono JS, Terstappen LWMM. All circulating EpCAM+CK+CD45- objects predict overall survival in castration-resistant prostate cancer. *Ann Oncol Off J Eur Soc Med Oncol* 2010 Sep 1;**21**(9):1851-7 Internet. cited 2017 Nov 23. Available fromhttps://academic.oup.com/annonc/article-lookup/doi/10.1093/annonc/mdq030.
9. Nanou A, Coumans FAW, van Dalum G, Zeune LL, Dolling D, Onstenk W, et al. Circulating tumor cells, tumor-derived extracellular vesicles and plasma cytokeratins in castration-resistant prostate cancer patients. Oncotarget [Internet]. 2018 Apr 9 [cited 2018 Dec 7];9(27):19283–93. Available from: http://www.oncotarget.com/fulltext/25019.
10. Wit S, Rossi E, Weber S, Tamminga M, Manicone M, Swennenhuis JF, et al. Single tube liquid biopsy for advanced non-small cell lung cancer. Int J Cancer [Internet]. 2019 Jun 15 [cited 2019 May 27];144(12):3127–37. Available from: https://onlinelibrary.wiley.com/doi/abs/10.1002/ijc.32056.
11. Buzás EI, Gardiner C, Lee C, Smith ZJ, Buzás EI, Gardiner C, et al. Single particle analysis: methods for detection of platelet extracellular vesicles in suspension (excluding flow cytometry). Platelets [Internet]. 2017;00(00):1–7. Available from: doi:10.1080/09537104.2016.1260704
12. Krafft C, Wilhelm K, Eremin A, Nestel S, Bubnoff N Von, Schultze-seemann W, et al. A specific spectral signature of serum and plasma-derived extracellular vesicles for cancer screening. Nanomedicine Nanotechnology, Biol Med [Internet]. 2016 [cited 2017 Aug 1];13:1–7. Available from: http://ac.els-cdn.com/S154996341630212X/1-s2.0-S154996341630212X-main.pdf?_tid=3240bc5a-769e-11e7-962c-00000aab0f02&acdnat=1501580928_2cf398639a64706b5b9501e9b256e2ad.
13. Carney RP, Hazari S, Colquhoun M, Tran D, Hwang B, Mulligan MS, et al. Multispectral optical tweezers for biochemical fingerprinting of cd9-positive exosome subpopulations. Anal Chem [Internet]. 2017 [cited 2018 Feb 12];89(10):5357–63. Available from: https://pubs.acs.org/doi/pdf/10.1021/acs.analchem.7b00017.
14. Smith ZJ, Lee C, Rojalin T, Carney RP, Hazari S, Knudson A, et al. Single exosome study reveals subpopulations distributed among cell lines with variability related to membrane content. J Extracell Vesicles [Internet]. 2015 [cited 2018 Aug 15];4(1):28533. Available from: http://www.ncbi.nlm.nih.gov/pubmed/26649679.
15. Kruglik SG, Royo F, Guigner J-M, Palomo L, Seksek O, Turpin P-Y, et al. Raman tweezers microspectroscopy of circa 100 nm extracellular vesicles. Nanoscale [Internet]. 2019;(January). Available from: https://pubs.rsc.org/en/Content/ArticleLanding/2019/NR/C8NR04677H#!divAbstract.
16. Lee W, Nanou A, Rikkert L, Coumans FAWW, Otto C, Terstappen LWMMMM, et al. Label-free prostate cancer detection by characterization of extracellular vesicles using Raman spectroscopy. 2018 [cited 2019 Mar 18];90:11. Available from: https://pubs.acs.org/sharingguidelines.

17. Penders J, Pence IJ, Horgan CC, Bergholt MS, Wood CS, Najer A, et al. Single particle automated raman trapping analysis. Nat Commun [Internet]. 2018 Dec 15 [cited 2019 Jun 7];9(1):4256. Available from: http://www.nature.com/articles/s41467-018-06397-6.
18. Ashkin A. Acceleration and trapping of particles by radiation pressure. Phys Rev Lett [Internet]. 1970 [cited 2018 Dec 4];24(4):156–9. Available from: https://journals.aps.org/prl/pdf/10.1103/PhysRevLett.24.156.
19. Ashkin A, Dziedzic JM, Chu S. Observation of a single-beam gradient force optical trap for dielectric particles. Opt Lett [Internet]. 1986 [cited 2018 Dec 4];11(5):288–90. Available from: https://www.osapublishing.org/DirectPDFAccess/C179D625-C7ED-5824-AC50C0B8F3390362_8652/ol-11-5-288.pdf?da=1&id=8652&seq=0&mobile=no.
20. Liu TH, Chiang WY, Usman A, Masuhara H. Optical trapping dynamics of a single polystyrene sphere: continuous wave versus femtosecond lasers. *J Phys Chem C* 2016;**120**(4):2392-9.
21. Ashkin A, Dziedzic JM. Optical trapping and manipulation of viruses and bacteria. Science [Internet]. 1987 Mar 20 [cited 2019 Jun 7];235(4795):1517–20. Available from: http://www.ncbi.nlm.nih.gov/pubmed/3547653.
22. Pang Y, Song H, Kim JH, Hou X, Cheng W. Optical trapping of individual human immunodeficiency viruses in culture fl uid reveals heterogeneity with single-molecule resolution. Nat Nanotechnol [Internet]. 2014;9(8):624–30. Available from: doi:10.1038/nnano.2014.140.
23. Rkiouak L, Tang MJ, Camp JCJ, McGregor J, Watson IM, Cox RA, et al. Optical trapping and Raman spectroscopy of solid particles. Phys Chem Chem Phys [Internet]. 2014 May 21 [cited 2018 Nov 15];16(23):11426–34. Available from: http://xlink.rsc.org/?DOI=C4CP00994K.
24. Chan JW, Winhold H, Lane SM, Huser T. Optical trapping and coherent anti-Stokes Raman scattering (CARS) spectroscopy of submicron-size particles. *IEEE J Sel Top Quantum Electron* 2005;**11**(4):858-63.
25. van der Pol E, Coumans FAW, Sturk A, Nieuwland R, van Leeuwen TG. Refractive index determination of nanoparticles in suspension using nanoparticle tracking analysis. 2014 Nov 12 [cited 2019 Mar 6];14(11):6195–201. Available from: http://pubs.acs.org/doi/10.1021/nl503371p.
26. Mätzler C. MATLAB functions for mie scattering and absorption version 2 [Internet]. 2002 [cited 2019 May 29]. Available from: http://www.atmo.arizona.edu/students/courselinks/spring09/atmo656b/maetzler_mie_v2.pdf.
27. Movasaghi Z, Rehman S, Rehman IU, Zanyar Movasaghi SR& DIUR. Raman spectroscopy of biological tissues. Appl Spectrosc Rev [Internet]. 2007 Sep 1 [cited 2018 Sep 19];42(5):493–541. Available from: http://www.tandfonline.com/action/journalInformation?journalCode=laps20.
28. M Rupert borah L, Mapar M, Vilas Shelke G, Norling K, Elmeskog M, Lo JO, et al. Effective refractive index and lipid content of extracellular vesicles revealed using optical waveguide scattering and fluorescence microscopy. Langmuir [Internet]. 2018 Jul 24 [cited 2018 Aug 14];34(29):8522–31. Available from: http://pubs.acs.org/doi/10.1021/acs.langmuir.7b04214.
29. Gardiner C, Shaw M, Hole P, Smith J, Tannetta D, Redman CW, et al. Measurement of refractive index by nanoparticle tracking analysis reveals heterogeneity in extracellular vesicles. J Extracell Vesicles [Internet]. 2014 [cited 2019 Jun 19];3(1). Available from: doi:10.3402/jev.v3.25361.
30. Konokhova AI, Yurkin MA, Moskalensky AE, Chernyshev A V., Tsvetovskaya GA, Chikova ED, et al. Light-scattering flow cytometry for identification and characterization of blood microparticles. J Biomed Opt [Internet]. 2012 [cited 2019 Jun 19];17(5):057006. Available from: http://biomedicaloptics.spiedigitallibrary.org/article.aspx?doi=10.1117/1.JBO.17.5.057006.
31. van der Pol E, de Rond L, Coumans FAW, Gool EL, Böing AN, Sturk A, et al. Absolute sizing and label-free identification of extracellular vesicles by flow cytometry. Nanomedicine Nanotechnology, Biol Med [Internet]. 2018;14(3):801–10. Available from: doi:10.1016/j.nano.2017.12.012.